Received: 27 April 2023 | Revised: 20 June 2023 | Accepted: 20 June 2023

DOI: 10.1111/jch.14694

ORIGINAL ARTICLE

WILEY

Deep gray matters iron deposition is positively associated with white matter hyperintensity in hypertension

Yu Su MD[1,2] | Wenjun Wu MD[1,2] | Ziji Qin MD[3] | Chungao Li MD[1,2] | Jie Zhao MD[1,2] | Jiamin Kang MD[1,2] | Youzhi Wang MD[1,2] | Chuansheng Zheng PhD[1,2] | Ewart Mark Haacke PhD[4,5] | Lixia Wang PhD[1,2]

[1]Department of Radiology, Union Hospital, Tongji Medical College, Huazhong University of Science and Technology, Wuhan, China

[2]Hubei Province Key Laboratory of Molecular Imaging, Wuhan, China

[3]Department of Radiology, The People's Hospital of Guangxi Zhuang Autonomous Region, Nanning, China

[4]Magnetic Resonance Innovations, Bingham Farms, Michigan, USA

[5]Department of Radiology, Wayne State University, Detroit, Michigan, USA

Correspondence
Lixia Wang, Department of Radiology, Union Hospital, Tongji Medical College, Huazhong University of Science and Technology, Wuhan, China.
Email: lisa2003627@163.com

Funding information
Hubei Provincial Key R&D Program, Grant/Award Number: 2022BCA034

Abstract

The association and underlying mechanisms between iron deposition and white matter hyperintensity (WMH) remain unclear. In this study, quantitative susceptibility mapping (QSM) was used to quantify deep gray matters iron deposition and to explore the association from both global and regional perspectives. A total of 84 patients with hypertension and 26 healthy controls underwent a strategically acquired gradient echo (STAGE) protocol, and the multi-echo data were used to reconstruct QSM images. The susceptibilities were used to describe iron content. Global region (RI) susceptibilities were measured in regions of interest, and age-related thresholds were used to determine high-iron content region (RII) susceptibilities. Compared with healthy controls, hypertension had higher total WMH scores and regional scores (all $p = .001$) and higher susceptibilities using the RI or RII analysis (all $p < .05$). In healthy controls, there was no significant association between susceptibilities and WMH scores. In hypertension, the susceptibilities of deep gray matters were positively correlated with WMH scores (RI analysis: right putamen; RII analysis: bilateral caudate nucleus head, putamen, red nucleus, substantia nigra, and dentate nucleus; age and education corrected $p < .05$). These findings suggest that iron deposition in deep gray matters was positively associated with WMH in hypertension, especially using the RII analysis.

KEYWORDS
high-iron content region, hypertension, iron, quantitative susceptibility mapping, white matter hyperintensity

Yu Su and Wenjun Wu contributed equally to this work.

1 | INTRODUCTION

Hypertension is a common chronic disease worldwide. It significantly affects the individual's health and increases the social economic burden. Hypertension currently affects about a quarter of Chinese, and the prevalence of grade 3 hypertension in older adults exceeds 5%.[1,2] Hypertension can damage the microvessels and lead to cerebral small vessel disease (cSVD).[3] White matter hyperintensity (WMH) tends to be the earliest manifestation and typical representative of cSVD, which is found in about 90% of the elderly over 60 years old.[4] Fluid-attenuated inversion recovery (FLAIR) or T2WI shows periventricular or deep WMH according to their location, and the histological changes include myelin loss, oligodendrocyte apoptosis, axonal injury, and/or astrogliosis.[5] Clinically, WMH-related cSVD is the common cause of neurodegeneration and vascular dementia.[6]

Cerebral non-heme iron including ferritin and hemosiderin is mainly stored in deep gray matters, and iron homeostasis is essential for the maintenance of physiological function. Excessive iron can damage neurons by promoting oxidative stress or ferroptosis,[7,8] and increased iron deposition has been detected in neurodegenerative diseases such as Alzheimer's and Parkinson's diseases.[9] Therefore, it is necessary to detect and quantify iron in the brain. Quantitative susceptibility mapping (QSM) has been proven to be a reliable and widely used method for brain iron quantification.[10] Several studies based on QSM have shown that hypertension is associated with iron deposition.[11,12] Meanwhile, previous studies found that iron deposition in gray matters was positively correlated with WMH,[13–15] but the specific mechanisms are still not understood completely. There was evidence that activation of endothelial cells and disruption of the blood-brain barrier (BBB) may be a common pathological basis for iron deposition and WMH.[16] Of note, a recent study in hemodialysis patients has identified WMH as a risk factor for iron deposition.[17] A hypertensive population based study may give new insight to the relationship between iron deposition and WMHs.

Most previous studies[14,15] on the relationship between iron deposition and WMH used a global region (RI) method to measure the susceptibilities, which cannot avoid the influence of diamagnetic substances to reduce the overall susceptibilities. Using a high-iron content region (RII) analysis can eliminate the impact of diamagnetic substances such as calcifications and sphingomyelins on iron assessment. In addition, RI analysis calculates the average susceptibilities of the brain region and cannot reveal the uneven distribution of iron.[18] Studies in healthy volunteers have demonstrated that the RII analysis is more robust and sensitive to reveal the linear relationship between iron and age.[19,20] Therefore, we hypothesize that a RII analysis would help us understand the association between iron deposition and WMH in a more precise way.

In this study, FLAIR and QSM were used to demarcate WMH and iron deposition, respectively. The aim was to explore the association between iron deposition and WMH using both the RI and RII analysis. This study provides a basis for further research on iron deposition and WMH-related neurodegenerative diseases.

2 | DATA AND METHODS

2.1 | Subjects

A cross-sectional approach was used in this study. The study protocol was approved by the Ethics Committee of our hospital. All subjects were willing to participate in this study and signed approved consent forms. From September 2019 to January 2022, a total of 117 patients with primary hypertension who were treated in our hospital were recruited. The diagnostic criteria for hypertension were defined as systolic blood pressure (SBP) ≥140 mmHg and/or diastolic blood pressure (DBP) ≥90 mmHg at rest or those who were taking antihypertensive drugs.[2] Exclusion criteria included: (1) secondary hypertension, such as renal hypertension or increased blood pressure due to endocrine disorders; (2) massive cerebral infarction, massive cerebral hemorrhage, brain tumor, and other obvious intracranial lesions or history of head surgery or trauma; (3) Alzheimer's disease, hepatolenticular degeneration, multiple sclerosis, Parkinson's disease, and other metabolic encephalopathies; (4) failed to complete the MRI examination or images with obvious artifacts; and (5) contraindications for an MRI examination. Finally, 34 patients were excluded by reference to the above criteria, and MRI data were available for a total of 84 patients, including 48 males and 36 females. All patients had hypertension for more than 1 year and were taking antihypertensive drugs regularly. Twenty-six healthy controls were matched by age and sex, and the clinical data of subjects were recorded.

2.2 | MRI data acquisition

All subjects underwent brain imaging on a 3.0 T magnetic resonance scanner (Siemens Healthcare, Skyra, Erlangen, Germany). Magnetic resonance images were acquired using a cranial 32-channel coil. Routine axial T1WI, FLAIR, and strategically acquired gradient echo (STAGE) sequences were performed. The specific parameters were: (1) Axial T1WI: TR/TE = 3570/165 ms, field-of-view (FOV) = 220 mm × 220 mm, matrix = 320 × 256, slice thickness = 6 mm, number of slices = 19; (2) Axial FLAIR: TR/TE = 9000/95 ms, FOV = 220 mm × 220 mm, matrix = 256 × 256, slice thickness = 6 mm, number of slices = 19. STAGE consisted of two double-echo gradient echoes with full flow compensation, and the parameters were as follows[21]: (1) Axial spin density weighted (PDW): TR = 25 ms, TE = 7.5/17.5 ms, FOV = 256 mm × 256 mm, flip angle = 6°, matrix = 384 × 144, voxel size = 0.67 × 1.33 × 2.0 mm^3, slice thickness = 2 mm, number of slices = 64; (2) Axial T1W: TR = 25 ms, TE = 8.75/18.75 ms, FOV = 256 mm × 256 mm, flip angle = 24°, matrix = 384 × 144,

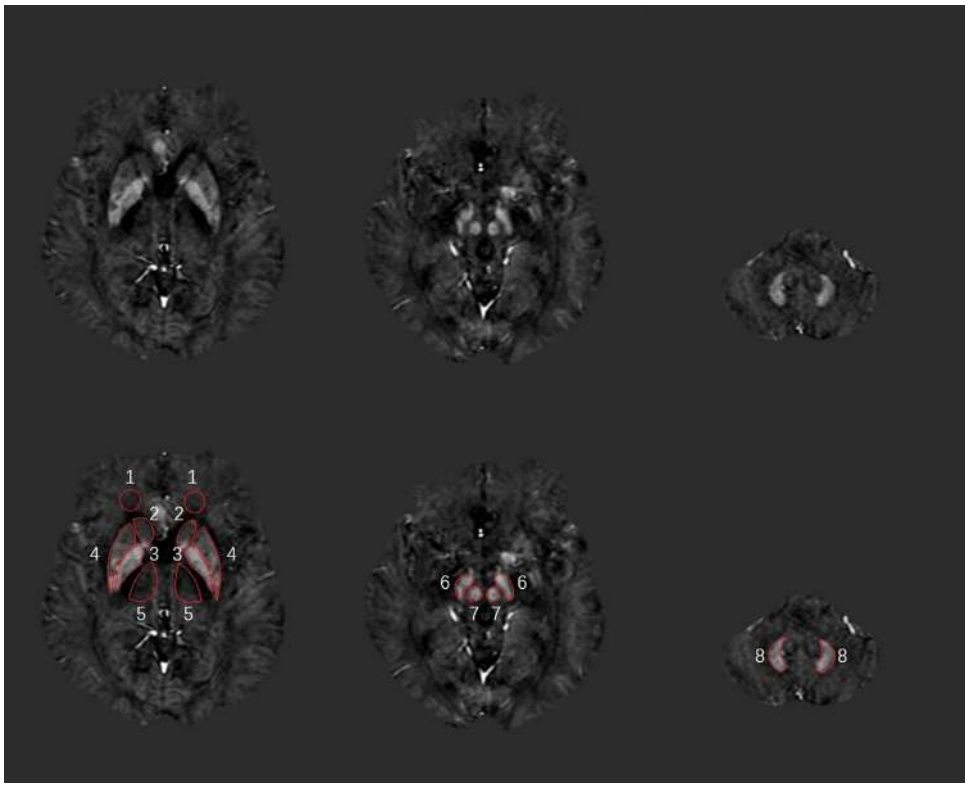

FIGURE 1 Upper row: Quantitative susceptibility mapping (QSM) of a 62-year-old male. Lower row: Region of, interest (ROI) was delineated on the QSM, including 1 = frontal white matter (FWM), 2 = caudate nucleus, head (CN), 3 = globus pallidus (GP), 4 = putamen (PU), 5 = thalamus (TH), 6 = substantia nigra (SN), 7 = rednucleus (RN), 8 = dentate nucleus (DN).

voxel size = 0.67 × 1.33 × 2.0 mm^3, slice thickness = 2 mm, number of slices = 64. The total acquisition time of STAGE was 5 min 36 s.

2.3 | MRI post-processing and measurement

The scanned PDW and T1W original images were transferred to the post-processing software of STAGE (version 2.1.4), and the phase images were used to reconstruct QSM. The processing steps[22,23] were: (1) application of the brain extraction tool (BET) for skull removal and phase unwrapping; (2) Removing the background field generated by the interface of air and tissue; (3) iterative susceptibilities weighted imaging and mapping (iSWIM) for QSM reconstruction from the pre-processed phase images.

Two trained neuroradiologists (W.W. with 6 years' experience and J.K. with 3 years' experience) delineated the regions of interest (ROI) according to the anatomy using the signal processing in nuclear magnetic resonance (SPIN) software (SpinTech MRI, Bingham Farms, MI). When delineating ROI, blood vessels and cerebrospinal fluid were avoided. Susceptibilities are given in ppb (parts per billion) and are relative to white matter. The ROI included bilateral caudate nucleus head (CN), putamen (PU), globus pallidus (GP), thalamus (TH), red nucleus (RN), substantia nigra (SN) and dentate nucleus (DN), and frontal white matter (FWM) (Figure 1). The average of the two neuroradiologists' measurements for each ROI was taken as the final RI susceptibilities. RII susceptibilities were automatically calculated based on the mean susceptibilities for a given age plus two standard deviations about the mean (Figure 2).[19,20]

2.4 | WMH scoring and grouping

WMH was scored by two neuroradiologists (W.W. with 6 years' experience and C.L. with 10 years' experience) according to the Fazekas scale.[24] Inconsistent results were determined by a third senior neuroradiologist (L.W. with 15 years' experience) after re-scoring. The periventricular WMH and deep WMH were scored separately, and the total scores were calculated by summation. The score criteria for periventricular WMHs were: 0: no lesions; 1: cap-like or line-like hyperintensity around the lateral ventricles; 2: the lesions of the anterior or posterior horn of the lateral ventricle showing smooth halo or paraventricular ribbon hyperintensity; and 3: diffuse paraventricular hyperintensity extending into deep white matter areas. The score criteria for deep WMH were: 0: no lesions; 1: punctate lesions; 2: patchy lesions or lesions beginning to confluence; and 3: extensive fusion of the lesions. According to the severity of WMH, hypertensive patients were divided into two groups: hypertensive with no WMH or mild WMH (n-m WMH, 0–2 scores) and hypertensive with moderate or severe WMH (m-s WMH, 3–6 scores).[25]

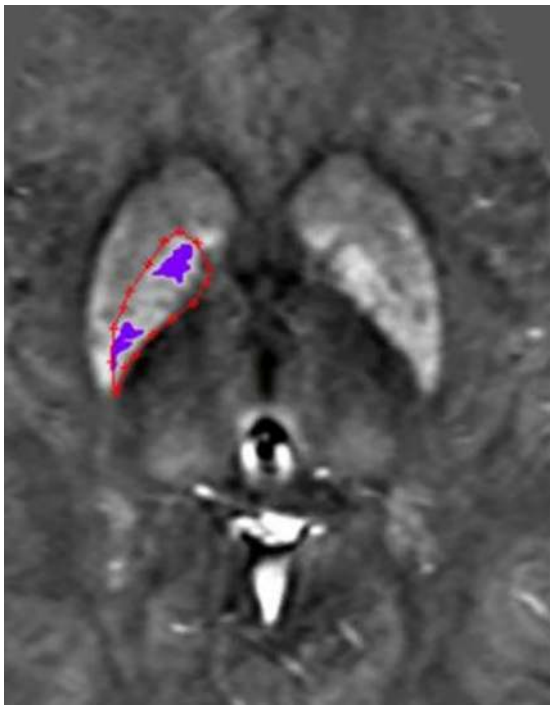

FIGURE 2 Diagram of the RI and RII region. The region inside the red line represents the RI of the right GP and, the purple region represents the distribution of the RII.

2.5 | Statistical analysis

All clinical data and susceptibilities were statistically analyzed using SPSS 25.0 (IBM, Chicago, IL, USA). The Shapiro–Wilk (S–W) method was used to test the normality of the quantitative data. According to the distribution characteristics of the data, the quantitative data were expressed as mean ± standard deviation (SD) or median with interquartile range separately. Frequency (%) was used to describe the categorical variables. The independent sample *t*-test, chi-square, or Wilcoxon Mann–Whitney test was used to compare the clinical data between healthy controls and hypertensive patients. The intra-class correlation coefficient (ICC) was used to test the consistency between the two neuroradiologists' measurements of susceptibilities. The paired t-test or independent sample *t*-test was separately used to compare the susceptibilities of bilateral hemispheres or the differences of the susceptibilities between the two groups. A covariance analysis with age as a covariate was calculated. To quantify the differences of susceptibilities between two groups, Cohen's *d* values were calculated as effect sizes. Age and education were selected as covariates, and partial correlation was used for the association between the susceptibilities and WMH scores. The hypertensiive patients were divided into two groups based on the mean age, the older (>61 years old) and the younger (≤61 years old) groups, and the association between susceptibilities and WMH scores was analyzed separately. The p value < .05 was considered significant.

TABLE 1 Clinical data of the two groups of subjects.

Variable	Healthy controls ($n = 26$)	Hypertension ($n = 84$)	p value
Age (years)	58.58 ± 6.16	61.27 ± 10.06	.103
Male (n, %)[a]	13 (50.0)	48 (57.1)	.522
BMI (kg/m^2)	24.53 ± 2.39	24.12 ± 3.34	.559
SBP (mmHg)	127.65 ± 18.67	139.50 ± 17.71	.004*
DBP (mmHg)	83.23 ± 11.17	83.47 ± 10.91	.923
Smoking (n, %)[a]	10 (38.5)	24 (28.6)	.340
Diabetes (n, %)[a]	1 (3.8)	16 (19.0)	.118
Education (years)[b]	9.0 (9.0, 12.0)	9.0 (6.0, 12.0)	.182
Hypertension duration (years)	–	8.5 (1.0, 13.0)	–
Classification of Hypertension (n, %)			–
1	–	14 (16.7)	
2	–	24 (28.6)	
3	–	46 (54.8)	
WMH scores	1.23 ± 0.99	2.54 ± 1.01	.001*
periventricular WMH scores	0.65 ± 0.69	1.45 ± 0.63	.001*
deep WMH scores	0.58 ± 0.50	1.08 ± 0.50	.001*

[a]The p value was obtained using the chi-square test.
[b]The p value was obtained using the Wilcoxon Mann-Whitney test.
*p value < .05.

3 | RESULTS

3.1 | Clinical data of subjects

There was no significant difference in age, gender, DBP, body mass index (BMI), smoking, diabetes, or education between the two groups. The SBP of hypertensive patients was significantly higher than healthy controls (p = .004). Compared with healthy controls, hypertensive patients had higher WMH scores, periventricular WMH scores, and deep WMH scores (all p = .001) (Table 1).

3.2 | Comparison of susceptibilities

The ICCs of RI susceptibilities between the two neuroradiologists were all >0.85 (right CN = 0.86, left CN = 0.93; right GP = 0.87, left GP = 0.92; right PU = 0.95, left PU = 0.94; right TH = 0.88, left TH = 0.88; right RN = 0.90, left RN = 0.90; right SN = 0.91, left SN = 0.89; right DN = 0.88, left DN = 0.92; right FWM = 0.91, left FWM = 0.86).

In hypertension, the susceptibilities of bilateral PU, and right DN increased compared with healthy controls in the RI analysis (all p < .05, Cohen's *d* values: .52–.98), and the RII analysis showed significant increase in bilateral PU, SN, DN, and left GP (all p < .05, Cohen's

TABLE 2 Comparison of RI and RII susceptibilities (ppb) in each brain region between the two groups.

	RI analysis				RII analysis			
Groups	Healthy Controls ($n = 26$)	Hypertension ($n = 84$)	p value	Effect size[a]	Healthy Controls ($n = 26$)	Hypertension ($n = 84$)	p value	Effect size[a]
Right CN	47.86 ± 9.16	48.98 ± 17.81	.673	0.08	86.05 ± 15.61	87.46 ± 15.75	.692	0.09
Left CN	42.73 ± 7.75	47.92 ± 20.96	.062	0.33	86.79 ± 9.98	87.56 ± 18.10	.784	0.05
Right GP	138.36 ± 26.21	153.11 ± 50.03	.153	0.37	195.57 ± 19.87	207.82 ± 37.48	.114	0.41
Left GP	140.76 ± 27.83	151.39 ± 48.96	.294	0.27	197.96 ± 18.57	209.84 ± 35.88	.029*	0.42
Right PU	52.77 ± 10.79	66.31 ± 27.76	.001*	0.64	102.87 ± 15.85	145.18 ± 34.45	.001*	1.58
Left PU	50.44 ± 13.28	68.68 ± 22.77	.001*	0.98	107.87 ± 13.65	138.60 ± 29.14	.001*	1.35
Right TH	−4.26 ± 6.80	−9.08 ± 8.82	.014*	−0.61	20.63 ± 5.24	18.78 ± 9.03	.198	−0.25
Left TH	−4.26 ± 6.80	−10.71 ± 9.31	.001*	−0.79	20.73 ± 4.04	18.22 ± 8.83	.164	−0.37
Right RN	133.83 ± 31.46	138.45 ± 35.98	.558	0.14	186.30 ± 14.79	194.29 ± 28.26	.063	0.35
Left RN	130.38 ± 29.79	134.18 ± 36.77	.631	0.11	183.24 ± 14.22	190.20 ± 27.22	.214	0.32
Right SN	146.59 ± 22.54	156.37 ± 34.69	.098	0.33	182.90 ± 14.04	207.17 ± 24.44	.001*	1.22
Left SN	149.32 ± 24.08	151.87 ± 33.99	.723	0.09	187.82 ± 12.31	204.31 ± 24.68	.001*	0.85
Right DN	114.49 ± 34.27	132.74 ± 35.63	.023*	0.52	165.87 ± 11.47	191.47 ± 22.56	.001*	1.43
Left DN	120.27 ± 30.75	131.67 ± 33.83	.128	0.35	166.19 ± 9.79	189.36 ± 22.24	.001*	1.35
Right FWM	−9.36 ± 3.57	−7.97 ± 6.46	.165	0.27	4.00 ± 8.55	2.53 ± 3.47	.399	−0.23
Left FWM	−9.40 ± 4.66	−7.99 ± 7.58	.257	0.22	3.48 ± 7.18	3.12 ± 3.82	.805	−0.06

*p value < .05.
[a]Cohen's d value.

d values: .42–1.35). Compared with healthy controls, the bilateral TH of hypertensive patients showed significantly lower susceptibilities in the RI analysis (all $p < .05$, Cohen's d values: −.61 and −.79), while there was no significant difference in the RII analysis (Table 2).

In n-m WMH, the susceptibilities of the left PU were slightly higher than that of the right ($p = .011$; Cohen's d value = −.19), and the susceptibilities of right RN were slightly higher than that of the left using RI analysis ($p = .038$; Cohen's d value = .14). In m-s WMH, there was no significant interhemispheric difference (Table 3). The RI analysis showed that the susceptibilities of each ROI in m-s WMH were higher than those of n-m WMH except for the bilateral TH and FWM, with significant differences in the bilateral GP, RN, and right SN (age corrected $p < .05$, Cohen's d values: .53–.73). The RII analysis showed that the susceptibilities of the bilateral GP, PU, RN, SN, and DN were significantly higher than those of n-m WMH (age corrected $p < .05$, Cohen's d values: .8-1.28) (Table 4).

3.3 | Correlation between susceptibilities and WMH scores

Age and years of education were controlled as covariates. There was no significant association between susceptibilities and WMH scores in healthy controls. In hypertension, the susceptibilities of the right PU were positively correlated with WMH scores in the RI analysis ($r = .264$, $p = .017$), and the susceptibilities of the bilateral CN, PU, RN, SN, and DN were positively correlated with WMH scores in the RII analysis(CN: left: $r = .376, p < .001$, right: $r = .239, p = .030$; PU: left: $r = .287, p = .009$, right: $r = .281$, $p = .010$; RN: left: $r = .255$, $p = .021$, right: $r = .277$, $p = .040$; SN: left: $r = .305$, $p = .005$, right: $r = .299$, $p = .006$; DN: left: $r = .314$, $p = .004$, right: $r = .324$, $p = .003$) (Figure 3).

The susceptibilities of the bilateral GP, PU, RN, SN, DN, and left CN were positively correlated with periventricular WMH scores, and the susceptibilities of the bilateral CN and PU were positively correlated with deep WMH scores in the RI or RII analysis (all $p < .05$) (Figure 4).

In the older group, the susceptibilities of the bilateral CN, PU, SN, DN, and left RN were positively correlated with WMH scores in the RI or RII analysis (all $p < .05$), and there was no significant correlation between the susceptibilities and WMH scores in the younger group (Figure 5).

4 | DISCUSSION

At present, the relationship between brain iron deposition and WMH is still controversial, and the mechanism remains not understood completely.[16] Our results showed that the susceptibilities of bilateral hemispheres' GP, PU, RN, SN, and DN were higher in m-s WMH compared to n-m WMH from global or regional perspectives, and the differences showed larger effect sizes using the RII analysis compared to RI analysis. Compared to previous studies,[13,14] this study used QSM combined with the RII iron quantification method and found iron deposition in more deep gray matters linking to WMH than RI analysis. Given the relationship between iron deposition and WMH,

TABLE 3 Comparison of RI susceptibilities (ppb) between the left and right hemispheres.

ROI	Left	Right	*p* value	Effect size[a]
n-m WMH				
CN	44.51 ± 13.19	47.17 ± 13.34	.124	0.20
GP	139.21 ± 40.98	138.70 ± 41.02	.851	−0.01
PU	64.53 ± 20.27	60.50 ± 22.31	.011*	−0.19
TH	−9.09 ± 8.32	−7.57 ± 6.71	.057	0.20
RN	125.55 ± 33.67	130.48 ± 35.67	.038*	0.14
SN	146.04 ± 36.59	149.27 ± 37.60	.315	0.09
DN	128.29 ± 29.58	130.76 ± 31.19	.283	0.08
FWM	−9.26 ± 8.02	−8.66 ± 6.39	.640	0.08
m-s WMH				
CN	52.93 ± 28.34	51.64 ± 22.83	.687	−0.05
GP	169.31 ± 54.60	174.30 ± 54.95	.150	0.09
PU	74.79 ± 25.10	74.86 ± 32.76	.981	0.01
TH	−13.11 ± 10.27	−11.29 ± 10.97	.197	0.17
RN	146.88 ± 37.93	150.16 ± 33.61	.341	0.09
SN	160.43 ± 28.12	166.81 ± 27.18	.078	0.23
DN	136.63 ± 39.20	135.65 ± 41.65	.759	−0.02
FWM	−7.12 ± 7.22	−7.51 ± 6.53	.687	0.06

p value was obtained using the paired *t*-test.
*p value <.05.
[a]Cohen's *d* value.

TABLE 4 Comparison of RI and RII susceptibilities (ppb) in each brain region between the two groups of hypertension.

	RI analysis					RII analysis				
Groups	n-m WMH ($n = 50$)	m-s WMH ($n = 34$)	*p* value	*P1* value	Effect size[a]	n-m WMH ($n = 50$)	m-s WMH ($n = 34$)	*p* value	*P1* value	Effect size[a]
Right CN	47.17 ± 13.34	51.64 ± 22.83	.675	.797	0.24	83.34 ± 12.47	93.51 ± 18.15	.006*	.330	0.65
Left CN	44.51 ± 13.19	52.93 ± 28.34	.312	.695	0.38	80.58 ± 11.76	97.82 ± 20.89	.001*	.067	1.02
Right GP	138.70 ± 41.02	174.30 ± 54.95	.002*	.010*	0.73	195.70 ± 23.05	225.64 ± 46.84	.001*	.033*	0.81
Left GP	139.21 ± 40.98	169.31 ± 54.60	.006*	.017*	0.62	197.31 ± 22.19	228.28 ± 43.79	.001*	.006*	0.89
Right PU	60.50 ± 22.31	74.86 ± 32.76	.019*	.427	0.51	131.31 ± 19.60	165.56 ± 41.17	.001*	.001*	1.06
Left PU	64.50 ± 20.27	74.79 ± 25.10	.042*	.697	0.45	126.74 ± 17.04	156.03 ± 34.34	.001*	.001*	1.08
Right TH	−7.57 ± 6.71	−11.29 ± 10.97	.083	.759	−0.41	19.35 ± 9.19	17.95 ± 8.86	.487	.240	−0.16
Left TH	−9.09 ± 8.32	−13.11 ± 10.27	.052	.925	−0.43	18.66 ± 8.91	17.57 ± 8.80	.580	.222	−0.12
Right RN	130.48 ± 35.67	150.16 ± 33.61	.013*	.027*	0.67	184.21 ± 17.62	209.11 ± 34.17	.001*	.003*	0.92
Left RN	125.55 ± 33.67	146.88 ± 37.93	.008*	.013*	0.59	184.21 ± 17.62	205.46 ± 33.39	.001*	.001*	0.80
Right SN	149.20 ± 37.60	166.80 ± 27.18	.022*	.045*	0.53	197.91 ± 13.41	220.80 ± 30.23	.001*	.001*	0.98
Left SN	146.04 ± 36.59	160.40 ± 28.12	.056	.083	0.44	194.94 ± 12.34	218.10 ± 31.26	.001*	.001*	0.97
Right DN	130.76 ± 31.19	135.65 ± 41.65	.540	.600	0.13	181.11 ± 12.38	206.71 ± 25.50	.001*	.001*	1.28
Left DN	128.29 ± 29.58	136.63 ± 39.20	.270	.931	0.24	179.15 ± 12.12	204.37 ± 25.22	.001*	.001*	1.27
Right FWM	−7.51 ± 6.53	−8.86 ± 6.39	.426	.565	−0.21	2.93 ± 3.35	1.93 ± 3.61	.198	.185	−0.29
Left FWM	−7.12 ± 7.22	−9.26 ± 8.02	.206	.361	−0.28	3.14 ± 3.32	3.08 ± 4.51	.941	.502	−0.02

P1 value: Analysis of covariance with age as a covariate.
*p value <.05.
[a]Cohen's *d* value.

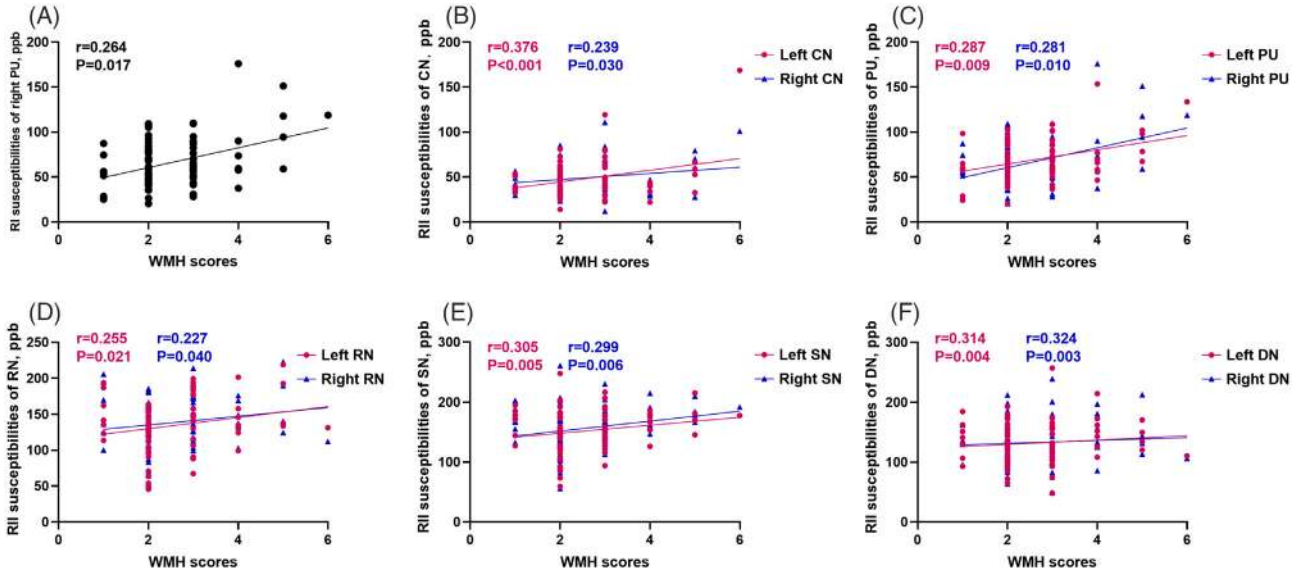

FIGURE 3 Diagram showing the partial correlation analysis between deep gray matters susceptibilities and WMH, scores. (A) Correlation between RI susceptibilities (right PU) and WMH scores. (B–F) correlation between RII, susceptibilities (bilateral CN, PU, RN, SN, and DN) and WMH scores.

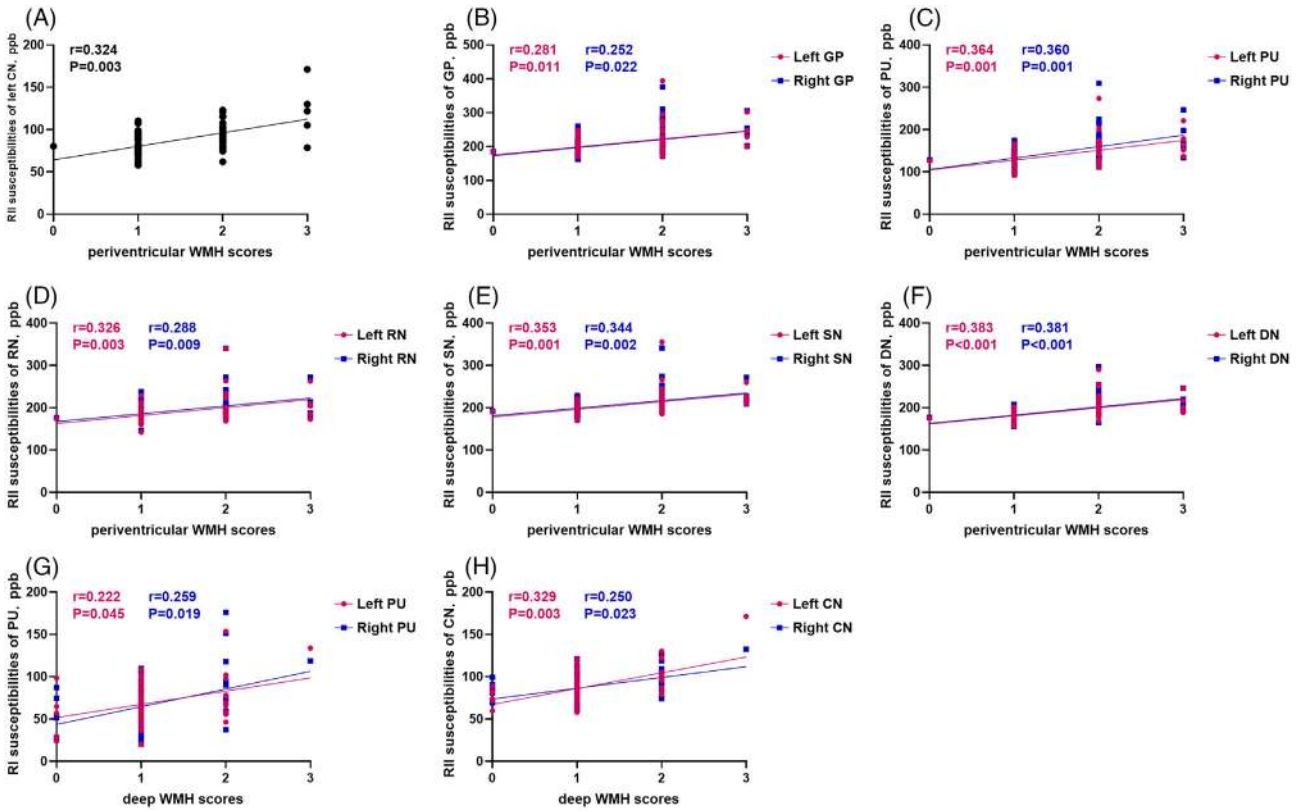

FIGURE 4 Diagram showing the partial correlation analysis between deep gray matters susceptibilities and, periventricular or deep WMH scores. (A–F) correlation between susceptibilities (bilateral GP, PU, RN, SN, DN, and left CN) and periventricular WMH scores. (G–H) correlation between susceptibilities (bilateral CN and PU), and deep WMH scores in the RI or RII analysis.

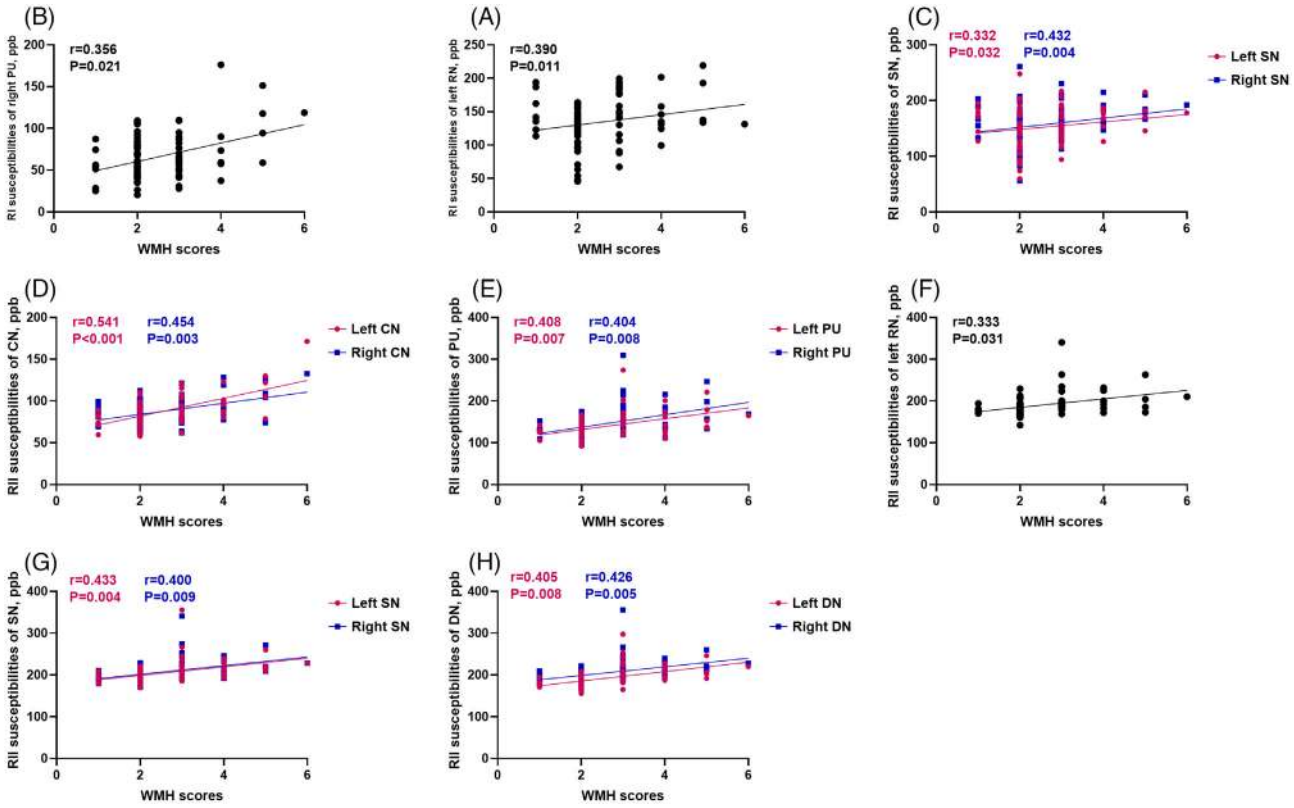

FIGURE 5 Diagram showing the partial correlation analysis between deep gray matters susceptibilities and WMH, scores in the older (>61 years old) group. (A–C) Correlation between RI susceptibilities (right PU, left RN, and, bilateral SN) and WMH scores. (D–H) Correlation between RII susceptibilities (bilateral CN, PU, SN, DN, and, left RN) and WMH scores.

they may share a common pathological basis or interact with each other.

Hypertension links to WMH and brain iron deposition, our results support this view. On the one hand, hypertension can cause and aggravate WMH through a variety of mechanisms such as ischemic injury and disruption of the BBB.[3,26] Also, hypertension-induced oxidative stress destroys the walls of microvessels and leads to increased permeability of the BBB and thereby promotes local tissue inflammation.[3,27] The secretion of inflammatory mediators such as hepcidin and NO affects iron transport and metabolism[28] and may result in a redistribution of iron in deep gray matters. Therefore, we speculate that cSVD caused by hypertension may be one of the potential causes of the correlation between WMH with iron deposition. Further analysis showed that iron deposition in more deep gray matters linked to periventricular WMH scores compared with deep WMH. Given the different sources of blood supply for different parts of the white matter, periventricular white matter is supplied by terminal arteries without collateral circulation and is more prone to ischemic injury.[5] In addition to the effects of hypertension, iron deposition and WMH also progress with aging.[4,9] Therefore, the correlation between them were more pronounced in the older group. Interestingly, we found that iron deposition of bilateral TH were lower in hypertension in the RI analysis, but no significant differences were found between hypertensive patients and healthy controls in the RII analysis, which may be attributed to the uneven distribution of iron in the TH.

Our results showed significant associations between WMH and iron deposition in CN, PU, RN, SN, and DN. A quantitative MRI study found that iron content in the basal ganglia (PU, GP, and CN) was positively correlated with the amount of anatomically linked white matter myelin in macaques, suggesting that iron may be involved in myelin synthesis.[29] Hill et al.[30] hypothesized that iron transported to neurons by transferrin could be transported along axons to terminal regions and be released or stored in oligodendrocytes. Therefore, we speculate that iron deposition in the deep gray matters may be partially caused by the disruption of iron transport by hypertension-related WMH. Moreover, the demyelination of white matter may decrease the demand for iron from the deep gray matters.[31] Iron accumulates with age and if not in a protective form such as ferritin or hemosiderin, can lead to the production of oxygen free radicals causing oxidative damage to neurons and other cells,[9] which may be the prodromal stage of WMH. In addition to myelin damage, Bauer et al.[15] thought that iron deposition of the basal ganglia may lead to the Wallerian degeneration of deep white matter tracts. Therefore, we speculate that iron deposition and WMH promote each other.

We found that the susceptibilities measured by RII analysis differed in more deep gray matters than RI analysis between hypertensive patients and healthy controls or m-s WMH and n-m WMH, suggesting that RII analysis may be an appropriate method to detect changes in iron content. Previous studies on Parkinson's disease and type 2 diabetes mellitus (T2DM)[18,32] have also shown that RII analysis is

more sensitive for distinguishing patients from healthy volunteers. Therefore, we speculate that RII analysis can reveal the correlation between iron deposition and WMH more sensitively, mainly due to: (1) removing interference from diamagnetic substances; and (2) better reflecting small-scale iron accumulation within the ROI or the uneven distribution of iron.[18]

There were relatively few studies on the relationship between iron deposition and WMH, and the results were inconsistent. One group used an R2* technology and found a positive correlation between iron deposition in GP and WMH volume of healthy adults.[13] However, Gattringer et al.[33] also used the R2* technology to analyze patients with transient neurological attacks and concluded that there was no correlation between iron deposition and the WMH volume. Another study[14] reported that iron deposition in the GP, PU, TH, and amygdala was positively correlated with WMH volume, but the relevant deep gray matters were not completely consistent with our results. We attribute the inconsistent results to different quantitative methods of iron deposition (QSM vs. R2*-MRI, RI vs. RII analysis) and different target subjects. Therefore, further studies are needed to clarify how WMH links to iron deposition in specific deep gray matters in specific populations. In addition, we found that the distribution of iron deposition in the PU and RN of the left and right hemispheres was asymmetric. The asymmetric distribution of iron may be related to human motor lateralization and motor control.[34] However, the effect sizes of the hemisphere's differences were small, and large hypertensive population based studies are needed to exclude sampling errors.

This study has several limitations. Firstly, this was not a longitudinal follow-up study to reveal a causal relationship between iron deposition and WMH. Secondly, the sample size for hypertension included in this study was relatively small, and only two age based subgroups were analyzed. Age-based stratified analysis may give further insight into underlying mechanism.[19] Thirdly, visual scoring, rather than quantitative measurements, was used for white matter assessment, which was more practical but less accurate. Therefore, further prospective cohort studies with larger sample sizes and broader quantitative assessments are needed for understanding the relationship between iron deposition and WMH.

5 | CONCLUSIONS

Both iron deposition in deep gray matters and WMH were aggravated in hypertension, and iron deposition increased with WMH. RII analysis revealed iron deposition in more deep gray matters linking to WMH than RI analysis. The positive association between iron deposition and WMH in hypertension may be based on common mechanisms of small vessel disease or underlying interaction.

ACKNOWLEDGMENTS

The research was supported by the Hubei Provincial Key R&D Program(Grant number: 2022BCA034)

CONFLICT OF INTEREST STATEMENT

The authors have no conflict of interest to declare.

INFORMED CONSENT STATEMENT

All participants signed approved consent forms and agreed to the publication of the article.

DATA AVAILABILITY STATEMENT

The data that support the findings of this study are available from the corresponding author upon reasonable request.

ORCID

Lixia Wang PhD https://orcid.org/0000-0003-0494-2735

REFERENCES

1. Wang JG, Zhang W, Li Y, Liu L. Hypertension in China: epidemiology and treatment initiatives. *Nat Rev Cardiol*. 2023. doi:10.1038/s41569-022-00829-z
2. Wang Z, Chen Z, Zhang L, et al. Status of hypertension in China: results from the China Hypertension Survey, 2012–2015. *Circulation*. 2018;137(22):2344-2356.
3. Ungvari Z, Toth P, Tarantini S, et al. Hypertension-induced cognitive impairment: from pathophysiology to public health. *Nat Rev Nephrol*. 2021;17(10):639-654.
4. Joutel A, Chabriat H. Pathogenesis of white matter changes in cerebral small vessel diseases: beyond vessel-intrinsic mechanisms. *Clin Sci (Lond)*. 2017;131(8):635-651.
5. Wu X, Ya J, Zhou D, Ding Y, Ji X, Meng R. Pathogeneses and imaging features of cerebral white matter lesions of vascular origins. *Aging Dis*. 2021;12(8):2031-2051.
6. Ottoy J, Ozzoude M, Zukotynski K, et al. Vascular burden and cognition: mediating roles of neurodegeneration and amyloid PET. *Alzheimers Dement*. 2023;19(4):1503-1517.
7. Yan N, Zhang JJ. The emerging roles of ferroptosis in vascular cognitive impairment. *Front Neurosci*. 2019;13:811.
8. Petrova J, Manolov V, Vasilev V, Tzatchev K, Marinov B. Ischemic stroke, inflammation, iron overload - Connection to a hepcidin. *Int J Stroke*. 2016;11(1):NP16-NP17.
9. Ward RJ, Zucca FA, Duyn JH, Crichton RR, Zecca L. The role of iron in brain ageing and neurodegenerative disorders. *Lancet Neurol*. 2014;13(10):1045-1060.
10. Langkammer C, Schweser F, Krebs N, et al. Quantitative susceptibility mapping (QSM) as a means to measure brain iron? A post mortem validation study. *Neuroimage*. 2012;62(3):1593-1599.
11. Li X, Jin D, Zhu Y, et al. Quantitative susceptibility mapping to evaluate brain iron deposition and its correlation with physiological parameters in hypertensive patients. *Ann Transl Med*. 2021;9(20):1582.
12. Qin Z, Wu W, Liu D, et al. Quantitative susceptibility mapping of brain iron relating to cognitive impairment in hypertension. *J Magn Reson Imaging*. 2022;56(2):508-515.
13. Yan S, Sun J, Chen Y, Selim M, Lou M. Brain iron deposition in white matter hyperintensities: a 3-T MRI study. *Age (Dordr)*. 2013;35(5):1927-1936.
14. Murray KD, Uddin MN, Tivarus ME, et al. Increased risk for cerebral small vessel disease is associated with quantitative susceptibility mapping in HIV infected and uninfected individuals. *Neuroimage Clin*. 2021;32:102786.
15. Bauer CE, Zachariou V, Seago E, Gold BT. White matter hyperintensity volume and location: associations with WM microstructure, brain iron, and cerebral perfusion. *Front Aging Neurosci*. 2021;13:617947.

16. Valdés Hernández M, Allerhand M, Glatz A, et al. Do white matter hyperintensities mediate the association between brain iron deposition and cognitive abilities in older people? *Eur J Neurol*. 2016;23(7):1202-1209.
17. Wang H, Chai C, Wu G, et al. Cerebral blood flow regulates iron overload in the cerebral nuclei of hemodialysis patients with anemia. *J Cereb Blood Flow Metab*. 2023;43(5):749-762.
18. Hu R, Gao B, Tian S, et al. Regional high iron deposition on quantitative susceptibility mapping correlates with cognitive decline in type 2 diabetes mellitus. *Front Neurosci*. 2023;17:1061156.
19. Liu M, Liu S, Ghassaban K, et al. Assessing global and regional iron content in deep gray matter as a function of age using susceptibility mapping. *J Magn Reson Imaging*. 2016;44(1):59-71.
20. Ghassaban K, Liu S, Jiang C, Haacke EM. Quantifying iron content in magnetic resonance imaging. *Neuroimage*. 2019;187:77-92.
21. Chen Y, Liu S, Wang Y, Kang Y, Haacke EM. STrategically Acquired Gradient Echo (STAGE) imaging, part I: creating enhanced T1 contrast and standardized susceptibility weighted imaging and quantitative susceptibility mapping. *Magn Reson Imaging*. 2018;46:130-139.
22. Zhou L, Chen Y, Li Y, et al. Intracranial iron distribution and quantification in aceruloplasminemia: a case study. *Magn Reson Imaging*. 2020;70:29-35.
23. Zhang T, Tang R, Liu S, et al. Plaque characteristics of middle cerebral artery assessed using strategically acquired gradient echo (STAGE) and vessel wall MR contribute to misery downstream perfusion in patients with intracranial atherosclerosis. *Eur Radiol*. 2021;31(1):65-75.
24. Fazekas F, Chawluk JB, Alavi A, Hurtig HI, Zimmerman RA. MR signal abnormalities at 1.5 T in Alzheimer's dementia and normal aging. *AJR Am J Roentgenol*. 1987;149(2):351-356.
25. Yu F, Feng X, Li X, et al. Gut-derived metabolite phenylacetylglutamine and white matter hyperintensities in patients with acute ischemic stroke. *Front Aging Neurosci*. 2021;13:675158.
26. Ter Telgte A, van Leijsen EMC, Wiegertjes K, Klijn CJM, Tuladhar AM, de Leeuw FE. Cerebral small vessel disease: from a focal to a global perspective. *Nat Rev Neurol*. 2018;14(7):387-398.
27. Li J, Nguyen TD, Zhang Q, Guo L, Wang Y. Cerebral microbleeds are associated with increased brain iron and cognitive impairment in patients with cerebral small vessel disease: a quantitative susceptibility mapping study. *J Magn Reson Imaging*. 2022;56(3):904-914.
28. Urrutia PJ, Bórquez DA, Núñez MT. Inflaming the brain with iron. *Antioxidants (Basel)*. 2021;10(1):61.
29. Pu R, Wu Z, Yu W, et al. The association of myelination in the internal capsule with iron deposition in the basal ganglia in macaques: a magnetic resonance imaging study. *Quant Imaging Med Surg*. 2020;10(7):1526-1539.
30. Hill JM, Ruff MR, Weber RJ, Pert CB. Transferrin receptors in rat brain: neuropeptide-like pattern and relationship to iron distribution. *Proc Natl Acad Sci USA*. 1985;82(13):4553-4557.
31. Liem MK, Lesnik Oberstein SA, Versluis MJ, et al. 7 T MRI reveals diffuse iron deposition in putamen and caudate nucleus in CADASIL. *J Neurol Neurosurg Psychiatry*. 2012;83(12):1180-1185.
32. Ghassaban K, He N, Sethi SK, et al. Regional high iron in the substantia nigra differentiates Parkinson's disease patients from healthy controls. *Front Aging Neurosci*. 2019;11:106.
33. Gattringer T, Khalil M, Langkammer C, et al. No evidence for increased brain iron deposition in patients with ischemic white matter disease. *Neurobiol Aging*. 2016;45:61-63.
34. Xu X, Wang Q, Zhang M. Age, gender, and hemispheric differences in iron deposition in the human brain: an in vivo MRI study. *Neuroimage*. 2008;40(1):35-42.

How to cite this article: Su Y, Wu W, Qin Z, et al. Deep gray matters iron deposition is positively associated with white matter hyperintensity in hypertension. *J Clin Hypertens*. 2023;25:768-777. https://doi.org/10.1111/jch.14694